Investigation into the Effect of Speed Variation on the Growth of Wear-Type Rail Corrugation

P.A. Bellette, P.A. Meehan, P.A and W.J.T. Daniel

CRC for Railway Engineering and Technology (Rail CRC), School of Engineering, University of Queensland, Brisbane, Qld 4072, Australia

ABSTRACT

A feedback model for wear-type rail corrugation has been modified to account for vehicle speed variations over successive passages, so that the effect on corrugation amplitude growth can be investigated. The feedback model encapsulates the most critical interactions occurring between the wheel/rail structural dynamics, rolling contact mechanics and rail wear. Using this model, numerical and analytical investigations are performed to quantitatively identify the effect of deliberately changing the speed of successive vehicle passages in a statistically controlled manner. The effect of different initial track profiles on the results is also investigated. The results provide insight into a possible alternative means of retarding wear-type corrugation growth.

INTRODUCTION

Rail corrugation is a significant problem for the railway industry worldwide. The type of corrugation on which this paper focuses is known as wear-type rail corrugation and is a particular concern to industry. It is characterised by long (100-400mm) and short (25-80mm) wavelengths. Rail corrugation is a periodic irregularity that is observed to develop on the running surface of the rail with use. This irregularity grows in amplitude as a function of the number of passes, until removal by grinding is required to ameliorate the excessive noise, vibration and associated problems caused by the corrugated rail. This grinding is expensive and represents a substantial cost to the railway industry (Sato *et al.* 2002). There have been some techniques suggested to delay the onset of corrugations, such as rail hardfacing, but a reliable remedy, other than grinding, remains elusive.

The high cost associated with removing corrugations has motivated much research into the prediction and prevention of corrugation. Research in Germany (Hemplemann and Knothe, 1996), Sweden (Igeland and Ilias, 1997), Japan (Matsumoto *et al.*, 1996) and elsewhere has resulted in the development of simulation methods which make use of complex finite element simulations of the track dynamics along with numerical models of the rolling contact mechanics. These models are useful in that they have successfully modeled the development of corrugations and also led to the identification of behavior that is characteristic of corrugation formation. One shortcoming of such models is the excessive computational expense of performing parametric investigations into trends that may reduce corrugation formation. It is thought that this limitation may be overcome by simpler analytic models of corrugation formation.

Progress on analytical modelling of the growth of wear-type rail corrugation has been achieved by a number of authors over the past fifty years (see Sato *et al.* 2002 for a comprehensive review). Modern examples of such models can be found in the work of Bhaskar *et al.* (1997), Muller (2001) and Nielson (1999). Potential shortcomings of these models are described in Meehan *et al.* (2005) and include the lack of consideration of the effect of variable speed over successive vehicle passages.

The model described in this paper is a modification of the simple finite pass time delay model described in Meehan *et al.* (2005), and is similar to the infinite pass delay model used in Song and Meehan (2004). It has been altered in this paper so as to account for different train speeds on consecutive passes. This should not be confused with varying speed, i.e. accelerating or decelerating during each pass, which is not considered here. This model uses a multiple degree of freedom modal description of the wheel and rail dynamics, a linear contact mechanics model and a feedback mechanism where the rail profile exiting a wheel passage is fed into the next wheel-set passage. It allows for an investigation into any reduction in growth rate that may be achieved by using different pass speed distributions, for a range of initial track profiles. These results provide insight into a possible method for reducing corrugation growth.

CORRUGATION MODEL

Time Domain Model

The variable speed model used in this paper is an extension of the model used in Song and Meehan (2004). The system diagram for this feedback model can be seen in figure (1).

This model can generally be described in four stages, as seen in figure 1. The first stage (I) is where the initial rail profile excites the dynamic components of the wheel-rail system. This leads to a variation in contact forces, which in turn affects the contact mechanics (II). The variable contact mechanics leads to a variation in the wear process (III) and this worn rail profile is fed back into this system over successive passages (IV).

This general model was used in Meehan *et al.* (2005) to derive a model by considering a modal description of the dynamics (I), a linear contact mechanics model (II), the frictional work hypothesis to derive a wear relationship (III) and a finite passage delay for the feedback process (IV). A modal description of the wheel/rail dynamics was chosen because experimental and theoretical evidence has shown that the approximately constant corrugation pitch can be associated with a dominant mode of system vibration. This model considers only a vertical vibration mode, but could be extended to account for other modes. The contact mechanics model is
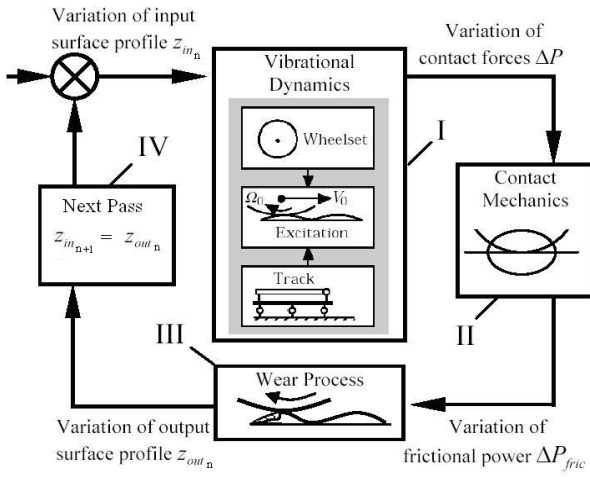
Figure 1. Feedback model for wear-type rail corrugation.

based on quasistatic microslip and considers small linear variations about nominal non-linear operating conditions (see Johnson, 1987). The dominant contributions for corrugation growth are assumed to come from the longitudinal components of traction, slip and wear. The wear model is based on assuming that the rate of wear is proportional to the frictional power dissipated.

In Song and Meehan (2004) this model was altered by considering an infinite time delay between passages (as is described in part IV of figure 1) to develop an analytic solution for multiple wheel-sets traversing a bump at the same speed. The present analysis follows a more general derivation, in that the speed may be different on successive passages. This allows insights to be gained into the effect of varying pass speeds for a wide range of initial track profiles. Note that finite time delay, as investigated in Meehan and Daniel (2004), has not been included in this paper to simplify the analysis and still provide insight into any possible growth rate reductions.

The equations that govern the modal wheel and rail dynamics (representing part I in figure 1) are given by,

$$\ddot{y}_i + 2\xi_i\omega_i\dot{y}_i + \omega_i^2 y_i = \frac{k_c}{m_i}(p_i - 1)z_{out_n}(a_n t), \qquad (1)$$

for $i = 1$ to M, where M is the number of modes and each y_i is a component of the modal displacement of the wheel/rail system. These relate to the actual wheel and rail displacement by,

$$y_w = \sum_{i=1}^{M} p_i y_i, \qquad (2)$$

and

$$y_r = \sum_{i=1}^{M} y_i. \qquad (3)$$

In these equations t represents time, ξ_i is the modal damping ratio, ω_i is the natural frequency, m_i is the modal mass, k_c is the contact stiffness, p_i is the modal contribution factor, z_{out} is the nth pass rail profile and a_n is the ratio of the nth pass speed to the average pass speed.

The equation that describes the wear and contact mechanics (parts II and III in figure 1) is given by,

$$z_{out_{n+1}}(t) = K_b\left(\sum_{i=1}^{M}\left[y_{i_{n+1}}\left(\frac{1}{a_n}t\right)(1-p_i)\right]\right) + \alpha z_{out_n}(t), \qquad 4)$$

where

$$\alpha = 1 + K_b, \qquad (5)$$

and

$$K_b = \frac{C_\xi k_c \Delta z_0}{P_0}, \qquad (6)$$

where C_ξ is the creep coefficient, Δz_0 is the steady state wear per pass and P_0 is the steady state contact pressure.

Transfer Function

If the Laplace transforms of (1) and (4) are taken then, after some manipulation, the relationship between the $(n+1)^{th}$ rail profile and n^{th} profile in Laplace Space can be shown to be given by,

$$Z_{n+1} = A_n Z_n, \qquad (7)$$

where

$$A_n = \alpha + \sum_{i=1}^{M}\left(\frac{-K_b K_{c_i}}{a_n^2 s^2 + 2\xi_i\omega_i a_n s + \omega_i^2}\right), \qquad (8)$$

and

$$K_{c_i} = \frac{k_c}{m_i}(1-p_i)^2. \qquad (9)$$

Here s represents the usual Laplace Space complex variable, and $Z(s)$ is the Laplace Transform of the rail profile $z(t)$.

A transfer function between the initial rail profile and the nth rail profile in Laplace Space can be derived by solving (7) for an initial profile Z_0 to give,

$$\frac{Z_n}{Z_0} = \prod_{k=1}^{n}\left(\alpha + \sum_{i=1}^{M}\left(\frac{-K_b K_{c_i}}{a_k^2 s^2 + 2\xi_i\omega_i a_k s + \omega_i^2}\right)\right). \qquad (10)$$

Note that equations (1) to (10) are similar to those developed in Song and Meehan (2004), except that the variable pass speeds result in a product over the number of passes in equation (10), the speed scaling factor a_k has been introduced and the sum over modes has been retained.

Frequency Response

To develop a method for quantifying the growth rate, the peak of the frequency response's amplitude ratio as a function of pass number (n) shall be investigated (the "H_∞ norm" encountered in modern control theory). This measure of corrugation growth is useful because it is relatively simple to derive the frequency response (using the transfer function (10)) and also that the H_∞ norm has useful properties relating to the magnitude of the corrugated profile when compared against the input profile (for example, it will be equal to the ratio of the induced (worst-case) 2-norms of the output and input profiles in the time domain (Skogestad and Postlethwaite, 1996), making it a useful, general measure of the expected corrugation amplitude).

This frequency response peak can also be interpreted in a more simple way as being related to the height of the highest peak of the Fourier Transform of the corrugated output profile (however caution should be taken with this assumption, as the transients generated from different initial profiles can have a large effect for a small number of passes, as is described in Song and Meehan (2004). These effects become less evident as the number of passes becomes large).

If the assumption is made that the modes in the transfer function (10) are independent, then the following expression for the amplitude ratio of the frequency response can be derived,

$$\left|\frac{Z_n}{Z_0}(i\omega)\right| = \alpha^n \sqrt{\prod_{k=1}^{n}\left(\frac{\left(\omega_i^2 - a_k^2\omega^2 - \frac{K_b K_{c_i}}{\alpha}\right)^2 + (2\xi_i\omega_i a_k\omega)^2}{\left(\omega_i^2 - a_k^2\omega^2\right)^2 + (2\xi_i\omega_i a_k\omega)^2}\right)}. \quad (11)$$

Probabilistic Speed Distribution

It is of interest to examine the behavior of this frequency response as the number of passes becomes large and when the speeds are distributed randomly. If the ratio of speeds, x, are distributed according to some probability distribution, $p(x)$, then the expected value of the frequency response can be evaluated. The expected value of a general function, $f(x)$, of a random variable, x, with a probability distribution, $p(x)$, is defined by,

$$E(f(x)) = \int_{-\infty}^{\infty} f(x)p(x)dx, \quad (12)$$

(See for example Galambos and Simonelli, 2004). The expected frequency response can now be derived by considering the ratio of successive passes, which, after some manipulation of equation (11), can be shown to be given by,

$$\left|\frac{Z_n}{Z_0}(i\omega)\right| = \alpha^n \sqrt{e^{\int_{-\infty}^{\infty}\ln\left(\frac{\left(\omega_i^2 - x^2\omega^2 - \frac{K_b K_{c_i}}{\alpha}\right)^2 + (2\xi_i\omega_i x\omega)^2}{\left(\omega_i^2 - x^2\omega^2\right)^2 + (2\xi_i\omega_i x\omega)^2}\right)p(x)dx}}, \quad (13)$$

The expected frequency response for a large number of passes can now be evaluated by performing the integral in equation (13), provided the modes are sufficiently independent.

ANALYTIC SOLUTIONS

The transfer function (10) allows the analytic solution to be formed for different initial profiles and for any chosen sequence of pass speeds. In this paper three different profiles are chosen that represent idealisations of what is found in practice; these profiles are a sinusoid, a step and an impulse.

Solution to Sine Initial Profile

A sinusoidal rail profile can be thought of as an approximation to a train traversing a previously corrugated rail. In the time domain a sinusoidal profile with arbitrary amplitude (A) and angular frequency (b) is given by,

$$z_{out_0}(t) = A\sin(bt). \quad (14)$$

In Laplace Space it can be shown that this becomes,

$$Z_0 = \frac{Ab}{s^2 + b^2}. \quad (15)$$

Now by multiplying transfer function (10) by initial profile (15), the solution to the nth pass profile can be found by performing a Heaviside expansion (assuming no two passes have exactly the same speed) and then performing an Inverse Laplace Transform. The solution can then be shown to be given by

$$z_{out_n}(t) = Ab\left\{ A_1 e^{-\left(\sqrt{-b^2}\right)t} + A_2 e^{\left(\sqrt{-b^2}\right)t} + \sum_{i=1}^{M}\left[\sum_{k=1}^{n}\frac{B_{k_i}}{a_k}e^{-\omega_i\left(\xi_i - \sqrt{\xi_i^2 - 1}\right)\frac{t}{a_k}} + \sum_{k=1}^{n}\frac{C_{k_i}}{a_k}e^{-\omega_i\left(\xi_i + \sqrt{\xi_i^2 - 1}\right)\frac{t}{a_k}}\right]\right\}, \quad (16)$$

where

$$A_1 = \lim_{s_c \to -\sqrt{-b^2}} w(s_c)\left(s_c + \sqrt{-b^2}\right), \quad (17)$$

$$A_2 = \lim_{s_c \to \sqrt{-b^2}} w(s_c)\left(s_c - \sqrt{-b^2}\right), \quad (18)$$

$$B_{k_i} = \lim_{s_c \to \frac{\xi_i\omega_i}{a_k} - \frac{\omega_i\sqrt{\xi_i^2 - 1}}{a_k}} w(s_c)\left(a_k s_c + \xi_i\omega_i + \sqrt{\xi_i^2 - 1}\right), \quad (19)$$

$$C_{k_i} = \lim_{s_c \to \frac{\xi_i\omega_i}{a_k} + \frac{\omega_i\sqrt{\xi_i^2 - 1}}{a_k}} w(s_c)\left(a_k s_c + \xi_i\omega_i - \sqrt{\xi_i^2 - 1}\right), \quad (20)$$

and

$$w(s_c) = \frac{1}{s_c^2 + b^2}\prod_{k=1}^{n}\left(\alpha + \sum_{i=1}^{M}\left(\frac{-K_b K_{c_i}}{a_k^2 s_c^2 + 2\xi_i\omega_i a_k s_c + \omega_i^2}\right)\right). \quad (21)$$

Equation (16) defines the time domain solution (which can be converted to the space domain solution through the mean velocity) for the whole rail profile for the nth pass. Note that the equations for the coefficients (17) to (20) may appear to go to zero, but the term in brackets will cancel with a term in the denominator of (21).

Solution to Step Initial Profile

A step initial profile can be thought of as an idealisation of a wheel-set traversing a finite step of a long duration, such as going from one rail section and then onto another that is at a slightly different height (perhaps due to a different rail material hardness). It can also be thought of as an initial displacement perturbation to the wheel-set on a flat section of track.

Mathematically this step profile in Laplace Space will be given by,

$$Z_0 = \frac{A}{s}, \quad (22)$$

where the step occurs at the time origin and A is the step height. Again by multiplying (10) by (22) the nth pass profile in Laplace Space can be found, and by performing a Heaviside expansion and taking the Inverse Laplace transform, the time domain solution can also be found, giving,

$$z_{out_n}(t) = A \left\{ \frac{A_1}{s} + \sum_{i=1}^{M} \left[\sum_{k=1}^{n} \frac{B_{k_i}}{a_k} e^{-\omega_i\left(\xi_i - \sqrt{\xi_i^2-1}\right)\frac{t}{a_k}} \right. \right. \qquad (23)$$
$$\left. \left. + \sum_{k=1}^{n} \frac{C_{k_i}}{a_k} e^{-\omega_i\left(\xi_i + \sqrt{\xi_i^2-1}\right)\frac{t}{a_k}} \right] \right\},$$

where in this case

$$A_1 = \lim_{s_c \to 0} w(s_c)s_c, \qquad (24)$$

$$B_{k_i} = \lim_{s_c \to \frac{\xi_i \omega_i}{a_k} - \frac{\omega_i \sqrt{\xi_i^2-1}}{a_k}} w(s_c)\left(a_k s_c + \xi_i \omega_i + \sqrt{\xi_i^2-1}\right), \qquad (25)$$

$$C_{k_i} = \lim_{s_c \to \frac{\xi_i \omega_i}{a_k} + \frac{\omega_i \sqrt{\xi_i^2-1}}{a_k}} w(s_c)\left(a_k s_c + \xi_i \omega_i - \sqrt{\xi_i^2-1}\right), \qquad (26)$$

and

$$w(s_c) = \frac{1}{s_c} \prod_{k=1}^{n} \left(\alpha + \sum_{i=1}^{M} \left(\frac{-K_b K_{c_i}}{a_k^2 s_c^2 + 2\xi_i \omega_i a_k s_c + \omega_i^2} \right) \right). \qquad (27)$$

Solution to Impulse Initial Profile

The last profile to be considered is an impulse profile. This is an idealisation of a wheel-set traversing a small bump or dip of finite duration, such as going over a small weld. Mathematically this will be represented as a delta function, which for convenience will be set at the time origin.

It can be shown that the impulse profile solution will be equal to the time derivative of the time-domain step solution, the only difference being that in this case the coefficient A in equation (23) will be given by,

$$A = \int_{-\infty}^{\infty} \delta(t) dt \cdot \qquad (28)$$

Thus the solution will be given by,

$$z_{out_n}(t) = A \left\{ A_1 \delta_0(t) \right. $$
$$\left. - \sum_{i=1}^{M} \left[\sum_{k=1}^{n} \frac{\omega_i\left(\xi_i - \sqrt{\xi_i^2-1}\right) B_{k_i}}{a_k^2} e^{-\omega_i\left(\xi_i - \sqrt{\xi_i^2-1}\right)\frac{t}{a_k}} \right. \right. \qquad (29)$$
$$\left. \left. + \sum_{k=1}^{n} \frac{\omega_i\left(\xi_i + \sqrt{\xi_i^2-1}\right) C_{k_i}}{a_k^2} e^{-\omega_i\left(\xi_i + \sqrt{\xi_i^2-1}\right)\frac{t}{a_k}} \right] \right\},$$

where the coefficients are the same as those given in equations (24) to (27).

RESULTS

The first part of the results section will detail the correlation between these analytic solutions and the outputs given by a numerical straight track simulation, which is described in Meehan *et al.* (2003), where both models use two modes. The second part will show the growth rate reduction predicted by (13) for three sample probability distributions.

Comparisons with Numerical Simulations

To compare the analytic solutions with numerical simulations, the same sequence of randomly generated pass speeds were used in both the numerical model and the analytic

model. The coefficients used were generated from realistic physical data, as shown in table 1. The Fourier Transforms of these profiles were then taken, so that the frequency content of the signals could be compared. Some sample plots can be seen in figures (2), and (3). These plots show the results obtained for the rail profile in space and frequency domains by using an impulse initial profile. The plots also show speed distributions with different standard deviations in speed, to highlight the effect that speed distribution has on growth rate. Plots of the numerical and analytic solutions are shown overlaid; note that the high degree of correlation makes it difficult to discern the difference between the analytic and numerical solutions.
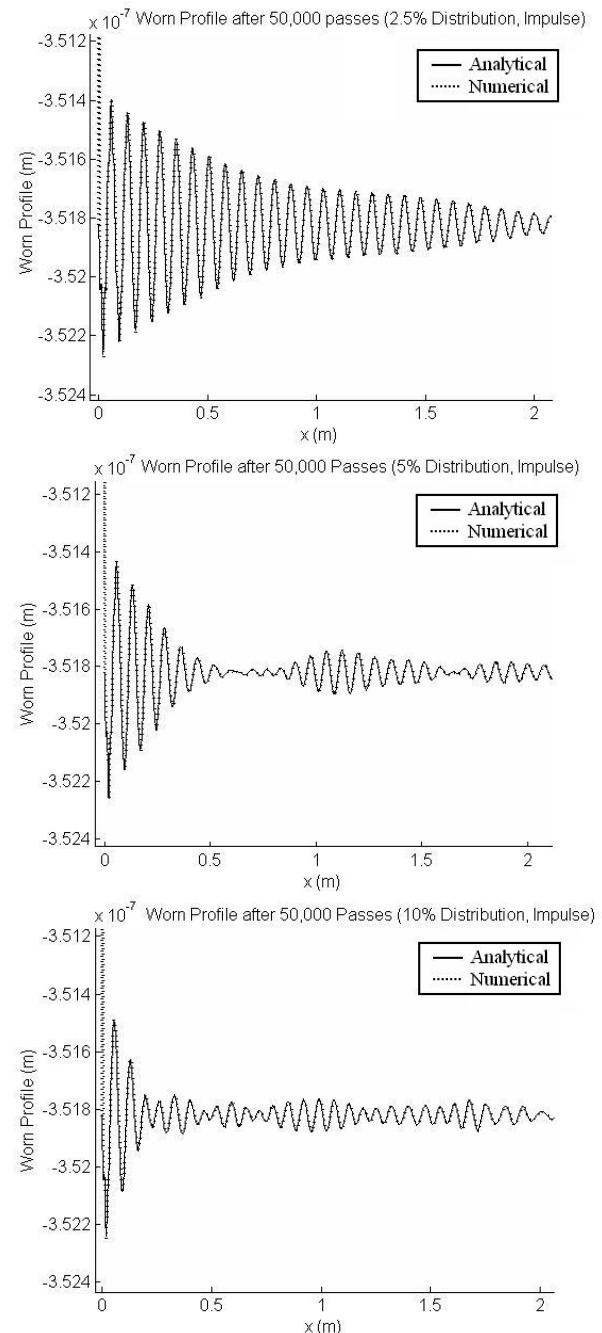
Figure 2. Rail Profile Numerical and Analytic Solutions for Impulse Profile after 50,000 passes. (a) 2.5%, (b) 5% and (c) 10% standard deviation in speed distribution.

Table 1. Railway Parameters for Simulation

Mean speed (m/s)	22.22	Track length (m)	6
Wheel mass (kg)	350	Rail density (kg/m)	7700
Wheel radius (m)	0.46	Rail Radius (m)	0.3
Wheel load (kN)	66	Coef. of friction	0.4
Young's Modulus (Steel) (N/m^2)	2.1×10^{11}	Primary rail damping ratio	0.01
Poisson's Ratio	0.3	Contact damping ratio	0.0021
Shear Modulus (Pa)	7.7×10^{10}	Sleeper spacing (m)	0.6
Sine amplitude (m)	1×10^{-9}	Sine wavelength (m)	0.025
Bump length (m)	0.001	Bump height (m)	1×10^{-6}
Step height (m)	1×10^{-7}	Wear coef. (kg/Nm)	1×10^{-6}
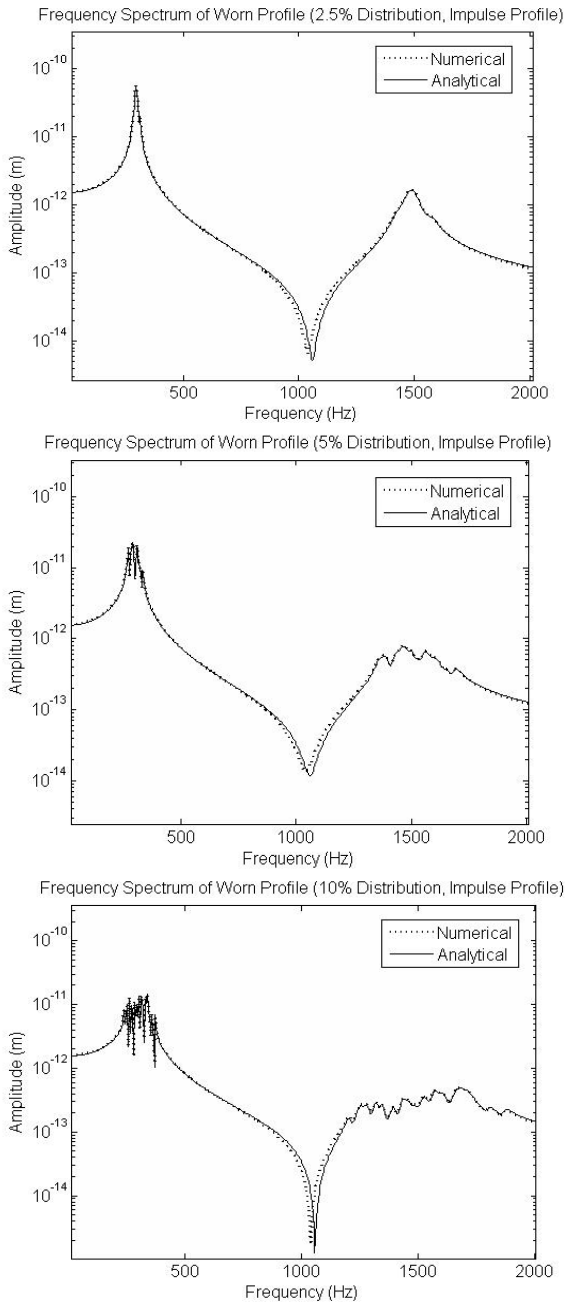
Figure 3. Frequency Spectra of Rail profile after 50,000 passes. (a), (b) and (c) are as in figure 2.

These plots give a good indication of typical results obtained when comparing these analytical solutions to results from the numerical simulator for the sinusoidal and step profiles, which have been omitted for the sake of brevity. The high correlation between these results gives confidence in the validity of both the numerical method used and of the approximations used to derive the analytic solution.

To show more detail of the frequency spectra plots and also to highlight the interesting effect that speed distribution has on the growth rate of corrugations, figures (4), (5) and (6) show the low frequency peak (at approximately 300Hz) of the Fourier Transform of the output profile for a sequence of normally distributed speeds but with each having a different standard deviation. This peak was chosen as it is the largest peak due to the dynamic wear. It can be seen that for all the initial profiles considered the same trend is observed that the larger the standard deviation the lower the growth rate. This is investigated further in the next section.
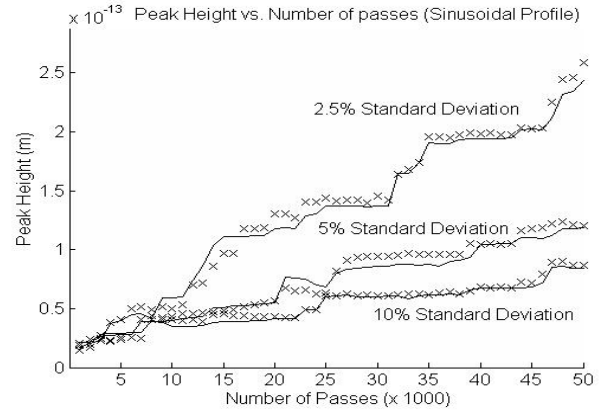
Figure 4. Peak of Frequency Spectra for a sinusoidal initial profile, for three different speed distributions.
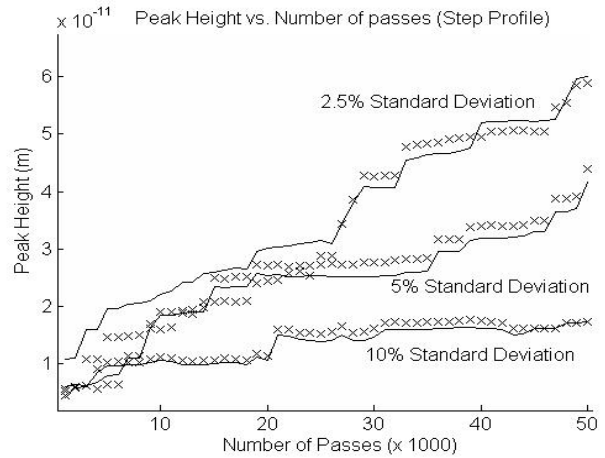
Figure 5. Peak of Frequency Spectra for a step initial profile for, three different speed distributions.
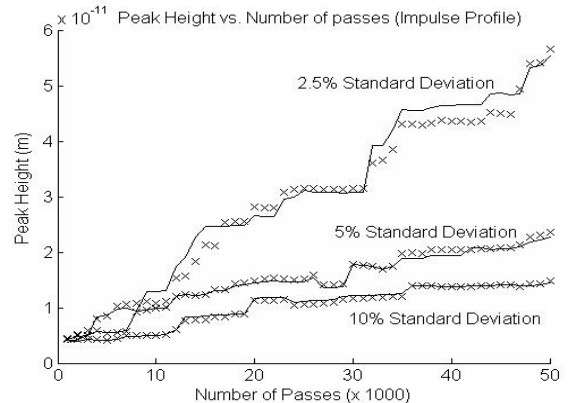
Figure 6. Peak of Frequency Spectra for an impulse initial profile, for three different speed distributions.

In figures (4), (5) and (6) there is some difference between the analytic and numerical peak height (particularly for the step profile for a 2.5% standard deviation speed distribution), most likely due to the resolution of the Fast Fourier Transform. Overall the numerical and analytic results show good agreement for the growth of the highest amplitude peak of the Fourier Transform.

Growth Rate Reduction

To find out the expected frequency response for a distribution of pass speeds, the integral in equation (13) can be evaluated either numerically or analytically. To investigate the growth rate reduction for different distribution properties, three different probability distributions have been examined. They are a uniform distribution, a triangular distribution and a normal distribution.

A uniform distribution gives an equal probability to all pass speeds within a certain range and is defined by,

$$p(x) = \frac{1}{c_2 - c_1} \quad \text{for } c_1 \le x \le c_2 , \tag{30}$$

and zero everywhere else.

A triangular distribution is defined by,

$$p(x) = \begin{cases} \dfrac{2(x-a)}{(b-a)(c-a)} & \text{for } a \le x \le c \\ \dfrac{2(b-x)}{(b-a)(b-c)} & \text{for } c \le x \le b \end{cases} , \tag{31}$$

and zero outside a and b. In (31) coefficient a represents the lower bound, coefficient b is the upper bound and coefficient c is the mode. In this paper triangular distributions that are symmetrical about the mode have been used.

A normal distribution is given by,

$$p(x) = \frac{1}{\sigma\sqrt{2\pi}} e^{\frac{-(x-\mu)^2}{2\sigma^2}} , \tag{32}$$

where σ is the standard deviation and μ is the mean.

To calculate the expected frequency response, equations (30), (31) and (32) can be used in equation (13) and the integral evaluated numerically. The peak of the frequency response, which shall be denoted by,

$$\left\| \frac{Z_n}{Z_{n-1}} \right\|_\infty = \sqrt[n]{\max_\omega \left| \frac{Z_n}{Z_0}(i\omega) \right|}, \tag{33}$$

can then be found and plotted against a distribution property. The growth rate G_r is then defined by,

$$G_r = \left\| \frac{Z_n}{Z_{n-1}} \right\|_\infty - 1, \tag{34}$$

as in Meehan *et. al.* (2005), and as stated previously we can relate this to the worst case ratio of the 2-norms of the output and input profile, which will grow like,

$$\left(\left\| \frac{Z_n}{Z_{n-1}} \right\|_\infty \right)^n = (1 + G_r)^n . \tag{35}$$

As mentioned previously, for some initial profiles (in particular an impulse profile or a corrugated profile with a frequency close to the expected resonant frequency of the system), this will also describe the growth of the peak of the frequency spectrum of the output profile.

To show the validity of this analysis, figure (7) shows the theoretically expected growth rate for a normal distribution versus the distribution's standard deviation (the solid line). Also plotted is the average growth rate obtained from numerical simulations, where an impulse initial profile has been used with the same parameters that are shown in table 1.
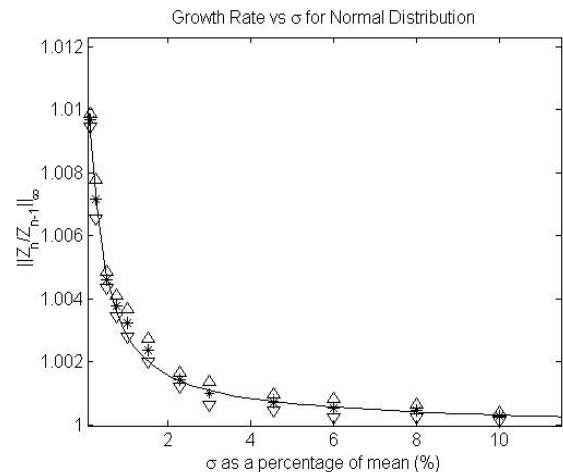
Figure 7. Growth Rate vs. Standard Deviation.

This growth rate was obtained by evaluating multiple runs of 100 accelerated wear passes (equivalent to 100,000 real passes), all generated with normally distributed pass sequences of a fixed standard deviation, and then averaging these growth rates. The mean growth rate from the numerical simulation is represented by the star and the triangle is the one standard deviation error bar. Similar plots have been obtained for triangular and uniform distributions. It can be seen that there is a good relationship between the theoretical growth rate and the growth rate obtained by the numerical simulations. Accelerated wear passes have been used (by artificially increasing the wear coefficient) because it significantly reduces computation times and introduces negligible error. Using equation (35) it can be shown that the error in this assumption can be approximated by,

$$\% \text{ error} \approx 100 \left(\frac{n}{2}(F-1) \right) G_r^2 , \tag{36}$$

where F is the wear acceleration factor. In these examples the maximum error induced by this assumption will be roughly 0.5%.

To show comparisons between these different distributions a common property of all the distributions is required. The two methods of comparison that have been examined in this paper are matching the variance of the three distributions and matching the width in which 95% of all passes will occur.

The variance is defined by,

$$\sigma^2 = \int (x - \mu)^2 P(x) dx , \tag{37}$$

where σ^2 is the variance and μ is the mean of the distribution. The variance can be thought of as the standard deviation squared.

Figure (8) shows the distributions when the variances are matched. Figure (9) shows the expected growth rate reduction for all three of these distributions when considering the variance.
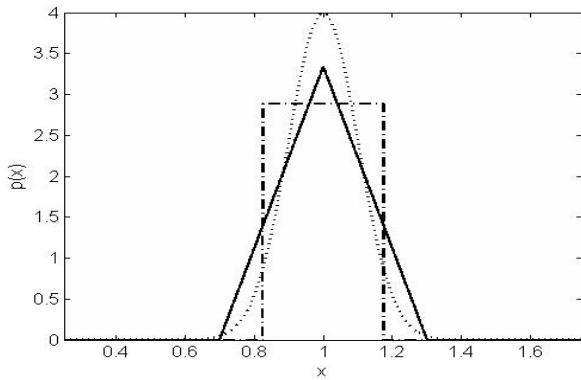
Figure 8. Probability Distributions with Matched Variance
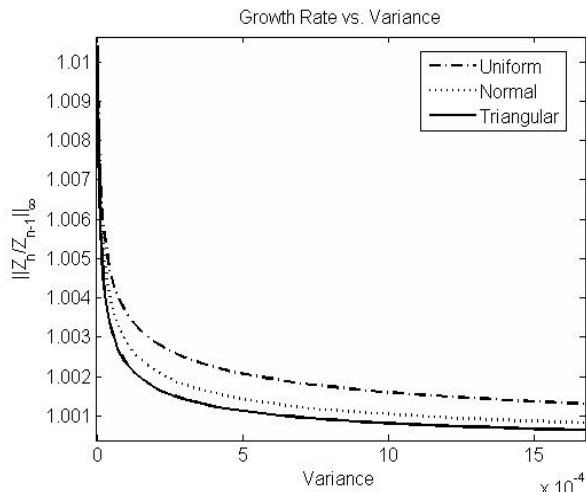
Figure 9. Growth rate vs. variance

All three distributions share the property that a wider variance results in a lower growth rate, with the greatest reduction being achieved by a triangular distribution and the lowest reduction given by the uniform distribution.

To serve as another basis for comparison of the growth rate reduction, the distributions were compared by matching the width in which 95% of passes will occur. This is intended to give a relative size comparison between the distributions. Figure (10) shows the three distributions with matched 95% width.
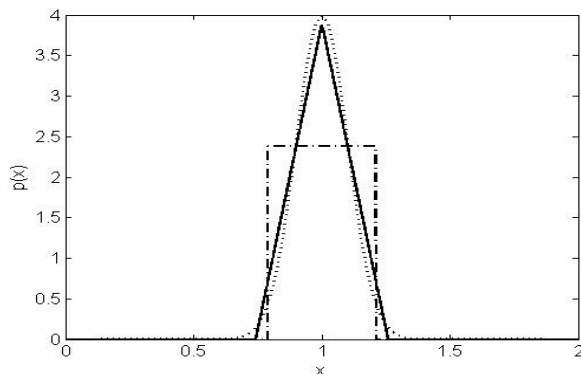
Figure 10. Probability Distributions with matched 95% width.

In figure (11), the growth rate reduction for the three distributions of equivalent width is shown, which follows the same trend as the matched variance case.
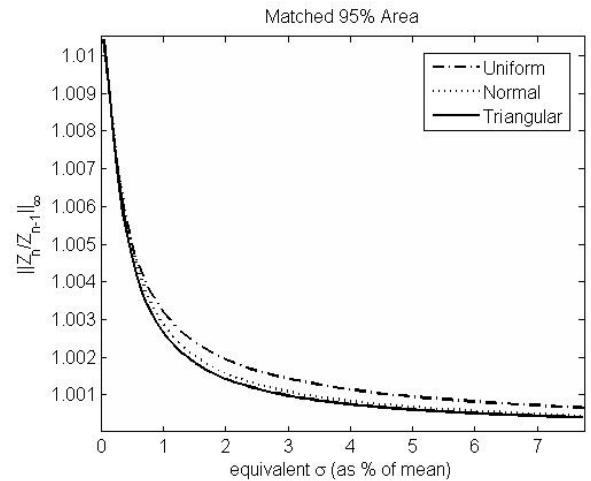
Figure 11. Growth rate vs. 95% width.

Figures (9) and (11) show that, for all the distributions considered, the theoretical growth rate can be reduced by a significant amount by increasing the "width" of the speed distributions. As an example of this, consider two sequences of normally distributed pass speeds, with the same mean, but 2% and 4% standard deviations. Using equation (35) and the data shown in figure (7), it can be shown that it will take approximately two times the number of passes for the corrugation amplitude to reach the same height. The same is approximately true for 4% and 8% standard deviations, etc. Thus a substantial reduction in the theoretical growth rate appears achievable.

It is observed that the broadness of the frequency response peak may reduce the effect of speed variation. This can be seen in figure (12) where the growth rate reduction for a normal distribution is plotted for various damping values. In this figure the damping used in table (1) has been increased by two and five times, broadening the frequency response.
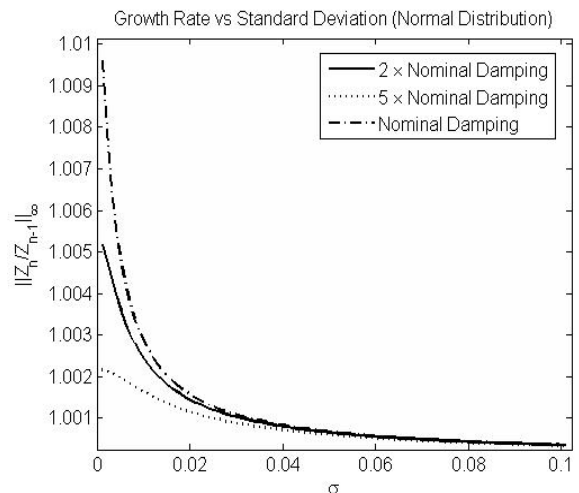
Figure 12. Growth rate vs. standard deviation for a range of damping values.

From this figure it can be seen that speed variation becomes less effective as the damping is increased. This effect can be more clearly seen if the predicted increase in grind interval is considered, that is the factor by which the theoretical time between grind intervals will be increased when compared against no speed variation. For example, if at a certain site

there is no speed variation and corrugations reach an amplitude that requires regrinding every year and then speed variation is introduced with a factor of increase f, it will now take f years for corrugations to reach the same amplitude. This factor of increase in grind interval is shown in figure 13.
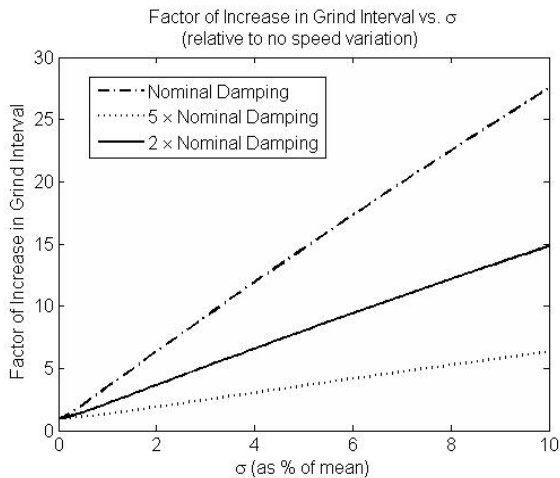
Figure 13. Factor of Increase in Grind interval (relative to no speed variation) vs. Standard Deviation for a range of damping values.

This shows that speed variation will increase the predicted grind interval by a considerable amount, even for the highly damped condition. As an example of the effectiveness of speed variation, the five times nominal damping example will still have a factor of increase in grind interval of approximately three for a 5% standard deviation in speed, which is considerably raised, which would result in grinding costs per annum being reduced to a third. It should also be noted that increasing the damping also reduces the growth rate when there is no speed variation, as discussed in Meehan *et al.* (2005)

CONCLUSIONS

An analytical solution for variable speed passes for three different initial rail profiles has been developed. These solutions show very good agreement with numerical simulations. The frequency spectra of these solutions, obtained by using a Fast Fourier Transform, are also in agreement. These solutions show that, for all the initial profiles considered, the properties of the probability distribution of speeds has a large effect on the growth rate of the corrugations. A frequency domain expression, derived from the analytic model using probability theory, shows good agreement with the numerical and analytical models and also allows for quantitative analysis of the growth rate reduction. Results of this analysis for realistic parameters indicate that substantial reductions in growth rate may be achieved by increasing the "width" of the speed distribution, such as by increasing the standard deviation. It has also been shown that increasing the breadth of the frequency response appears to make speed distribution less effective at reducing the growth rate, but large reductions in growth rate still occur.

A possible limitation of the approximate frequency response analysis is that it assumes that the modes are independent. Future work will include relaxing this assumption to examine what effect more complex linear response dynamics will have on the expected growth rate reduction. Another limitation of

the variable speed model as a whole is that it does not take account of non-linear behaviour, and is thus limited to small amplitude corrugation growth.

While these results show that there is a good correlation between analytical and numerical models, the validity when compared to real systems still needs to be evaluated. This will be tested in studies currently being planned, using both field data and an experimental test rig. Extensions of this work that are under consideration are the investigation of 3D cornering conditions and the effect on growth rate, the inclusion of a contact filter for short wavelengths and the inclusion of short, finite time delay effects.

ACKNOWLEDGEMENTS

REFERENCES

Bhaskar, A., Johnson, K.L., Wood, G.D. and Woodhouse, J., 1997, *Wheel-rail dynamics with closely conformal contact. Part 1. Dynamic modelling and stability analysis,* Proc. Inst. Mech. Eng. 211 (F), 11-26.

Galambos, J. and Simonelli, I., 2004, *Products of Random Variables*, Marcel Dekker, Inc., New York.

Hemplemann, K. and Knothe, K., 1996, An extended linear model for the prediction of short pitch corrugation, Wear 191, 161-169.

Igeland, A. and Ilias, H., 1997, Rail head corrugation growth predictions based on non-linear high frequency vehicle/track interaction, Wear 213, 90-97.

Johnson K.L., 1987, *Contact Mechanics*, Cambridge University Press, Cambridge.

Matsumoto, A., Sato, Y., Tanimoto, M. and Qi, K., 1996, *Study on the formation mechanism of rail corrugation on curved track,* Vehicle Sys. Dynam. 25, 450-465.

Meehan, P.A. and Daniel, W.J.T., 2004, *Wear-type rail corrugation prediction: passage time delay effects*, Proceedings of ACOUSTICS 2004, Gold Coast, Australia, 3-5 November, 11-16.

Meehan, P.A., Daniel, W.J.T. and Campey, T., 2003, *Wear-type rail corrugation prediction and prevention,* Proceedings of the 6th International Conference on Contact Mechanics and Wear in Rail/Wheel Systems (CM2003), Gothenburg, Sweden, June 10-13, 445-454.

Meehan, P.A., Daniel, W.J.T. and Campey, T., 2005, *Prediction of the growth of wear-type rail corrugation,* Wear 258, 1001-1013.

Muller, S., 2001, A linear wheel-rail model to investigate stability and corrugation on a straight track, Wear 249, 1117-1127.

Nielson, J.B., 1999, Evolution of rail corrugation predicted with a non-linear wear model, J. Sound Vibr. 227, 915-933.

Sato, Y., Matsumoto, A. and Knothe, K., 2002, *Review on rail corrugation studies*, Wear 253, 130-139.

Skogestad S. and Postlethwaite I., *Multivariable Feedback Control*, 1996, John Wiley and Sons, Chichester.

Song, N. and Meehan P.A., 2004, *A closed form analytical solution for a simplified wear-type rail corrugation model*, Proceedings of ACOUSTICS 2004, Gold Coast, Australia, 3-5 November, 227-232.